Geiger mode mapping: a new imaging modality for focused ion microprobes

Changyi Yang[1], Christiaan R. Hougaard[1], Edward Bielejec[2], Michael S. Caroll[2] and David N. Jamieson[1*]

[1]School of Physics, ARC Centre for Quantum Computation and Communication Technology, University of Melbourne, Parkville VIC 3010, AUSTRALIA.

[2]Sandia National Laboratories, POB 5800, Albuquerque, NM87185, USA.

*Corresponding author: d.jamieson@unimelb.edu.au

ABSTRACT

Geiger mode detectors fabricated in silicon are widely applied to detect incident photons with high sensitivity. They are operated with large internal electric fields so that a single electron-hole pair can trigger an avalanche breakdown which generates a signal in an external circuit. We have applied a modified version of ion beam induced charge in a nuclear microprobe system to investigate the application of Geiger mode detectors to detect discrete ion impacts. Our detectors are fabricated with an architecture based on the p-i-n diode structure and operated with a transient bias voltage that activates the Geiger mode. After the avalanche breakdown triggered by ion impact and diffusion of an electron-hole pair the avalanche breakdown is quenched by removal of the transient bias voltage which is synchronised with a beam gate. An alternative operation mode is possible at lower bias voltages where the avalanche process self-quenches and the device exhibits linear charge gain as a consequence. Incorporation of such a device into a silicon substrate potentially allows the exceptional sensitivity of Geiger mode to register an electron-hole pair from sub-10 keV donor atom implants for the deterministic construction of shallow arrays of single atoms only 10 nm deep in the substrate required for emerging quantum technologies. Our characterisation system incorporates a fast electrostatic ion beam switcher gated by the transient device bias, duration 800 ns, with a time delay, duration 500 ns, that allows for both the ion time of flight and the diffusion of the electron-

hole pairs in the substrate into the sensitive region of the device following ion impact of a scanned 1 MeV H microbeam. We compare images at the micron scale mapping the response of the device to ion impact operated in both Geiger mode and avalanche (linear) mode for silicon devices engineered with this ultimate-sensitivity detector structure.

1. INTRODUCTION

Silicon detectors engineered with the avalanche photo-diode (APD) architecture offer advantages for measuring low ionization energy and low numbers of e-h pairs compared with a traditional linear p-i-n photo-diode. APD detectors have many applications to photon measurement for the telecommunication industry and can be configured as linear sensors for the measurement of e-h pairs generated by photons [Campbell 2007, Tsujino 2007, Akiba 2005, Ghioni 2007], x-rays/gamma-rays [Baron 2000], energetic electrons [Kishimoto 2000] and ions [Yang 2010, Seamons 2008, Bielejec 2010]. APD devices operating in single-photon-counting mode have been successfully employed in several quantum key distribution (QKD) experiments [Kurtsiefer 2002, Schmitt-Manderbach 2007, Pelso 2009, Hughes 2002, Poppe 2004]. Hackers have exploited the vulnerability of APD devices to damage to induce a reduction in the charge gain and consequently compromise the security of QKD systems [Bugge 2014]. Therefore a detailed understanding of the charge injection and collection mechanisms in these ubiquitous devices is essential in many applications.

APD detectors can be biased to be operated in linear mode with charge gain (G) for the induced ionization with $1 < G < 100$. At higher bias voltages the APD can be operated in Geiger mode, in which a very high charge gain, $G > 1000$, can be established where the output signal can be triggered by a single e-h pair. We investigated signals from APD devices subject to ion impact with both Geiger mode ($G > 1000$) and linear mode ($1 < G < 10$) in a nuclear microprobe imaging analysis using 1 MeV He ions using the technique of ion beam induced charge (IBIC) [Yang 2010]. This follows from previous work on the characterisation of Si p-i-n detectors developed for deterministic doping of single donor devices [Morello 2010, Andresen 2000, Jamieson 2005, Hudson 2008, Mitic 2006].

These previous generation of devices provided a typical detection limit about 1 keV for the measurement of 3.5 keV ionization energy arising from single 14 keV P ion implants in the silicon substrate [Jamieson 2005] with a pre-fabricated 5 nm SiO_2 surface gate oxide. Under these conditions the ion placement accuracy is limited by ion straggling to about 11 nm, which strongly depends on the ion energy. Further improving the ion placement accuracy to sub-8 nm requires the use of sub-10 keV P ion, which produces much less ionization energy, near the detection limit of a p-i-n detector. Replacing the p-i-n detector design with the APD architecture in conjunction with thinner gate oxides provides an effective solution for implanting low energy ions (sub-10 keV) [Yang 2010, Seamons 2008, Bielejec 2010] and reduced ion implantation straggling uncertainty (~ 5-10 nm). APD devices operated in Geiger mode are very sensitive to optical beam damage. Similarly, the Geiger mode is also very sensitive to the ion beam damage, which can drastically reduce the charge gain in the device. This sets an upper limit to lifetime of the device. We applied 1 MeV He ions to map 2D signal distribution of the APDs configured in both Geiger mode and linear mode to measure the signal to noise ratio of the device for the detection of ion impacts.

2. EXPERIMENT

We investigated APDs fabricated at the Sandia National Laboratories designed to operate in Geiger mode using 1 MeV He^+ ions in the Melbourne nuclear microprobe. We recorded the signals from ion impact with the device operated in both the linear mode and the Geiger mode where the operating mode was determined by the bias voltage. For this purpose, a 1 pA 1 MeV He^+ beam was gated on for 1 microsecond per pulse, repeating with a 100 Hz cycle. The parameters are typical of a conventional IBIC experiment with an average beam intensity of ~ 1000 ions/sec for both Geiger and linear modes.

Owing to the differing nature of the signals from these modes, two different strategies were employed to interface the device to the data acquisition system. Figure 1 displays the systematic layout of the circuit diagrams for both Geiger mode and linear mode operation. In the Geiger mode

set-up (Figure 1a), synchronized gate pulses (ch-1 and ch-2) are provided by a Tektronix AFG3102 pulse generator. The gate pulse from ch-1 was sent to the APD to superimpose a bias voltage offset onto the DC bias voltage at the n^+-contact which raises the total bias voltage and activates the Geiger mode of operation. The gate pulse from ch-2 activated the fast ion beam switcher for beam-on-demand control. The delay between the two gate pulses was tunable to allow for the time of flight of the ions from the beam switcher to the target, the Geiger mode activation time and the diffusion of the ion-induced charge into the avalanche region of the device. For 1 MeV He ions, allowing for the time of flight from our switcher to the device (a distance of 9.5 m) and the charge drift time within the device of about 20 ns requires a delay time of 500 ns.

The interface of the device signals to the data acquisition system for Geiger mode operation, Figure 1a, is very different from that employed in linear mode, Figure 1b. This is because the output of the device operated in Geiger mode is a few tens mV in amplitude. Note that in contrast to the linear mode the output signal in Geiger mode does not depend on the magnitude of the ion induced ionization which triggers the avalanche process. The resulting current is sufficiently large that there is no need to use an amplifier. Instead a pulse discriminator was used to convert the Geiger signal directly from the device to a TTL pulse for the input into the data acquisition system. The timing of the various gates pulses and device signal are shown in Figure 2. This compares the waveforms of the bias offset (ch-1), beam gate pulse (ch-2) and the Geiger signal associated with a single ion strike in the device. The gate signals were configured so that the Geiger signal was generated from a single ion strike within the time window of Geiger mode activation. The device bias pulse could be delayed from 100 ns to 1200 ns after the leading edge of the ch-2 pulse controlling the beam deflector in order to find the optimum settings of operation so that the maximum signal from the ion impact could be detected in competition with the background dark signals.

For linear mode operation standard IBIC electronics was employed as shown in Figure 1b. The device was cooled down to 80 K temperature to reduce leakage current and the generation of thermal carriers in both Geiger and linear modes of operation.

We tested an APD device SHV1150 (photo in Figure 3), which was designed with a high field avalanche zone constructed under a n^+ contact disk surrounded with a guard-ring at its outer edge for smoothing the local field gradient at the electrode edge. The device was first tested with Geiger mode imaging. Maps of the output signals were obtained for four different delay times, 100 ns, 500 ns, 700 ns and 1200 ns, between the bias offset (ch-1) and the beam gate pulse (ch-2) .The Geiger mode maps with the individual delays are displayed and compared in Figure 3. For the purpose of these experiments, the device was not configured to minimize the background noise hence signals from thermal carriers are present at every pixel in the maps. However the signals from the ion impacts clearly reveal the central region of the device where the ion-induced Geiger signals are produced. By comparing the count rate from the background to the central region it is possible to find the signal to noise ratio as a function of the delay time. This is a maximum when the delay compensates for the various charge transport times and can be optimized still further by reduction in the gate widths to maximize the trade-off between live time, incident beam current and background noise at the operating temperature of the device.

After the completion of the Geiger mode imaging, linear mode IBIC imaging was performed with similar beam and device parameters and the data acquisition configured as shown in figure 1. In this mode the bias offset pulse was not used. The linear mode was found to have a charge gain of 1.4 (Figure 3) within the device central area which corresponds to the avalanche zone. Outside of the central area far away from the n^+ contact of the device there was no observation of avalanche charge multiplication showing the local internal fields were not strong enough to trigger an avalanche. We also observed that the device in Geiger mode was much more sensitive to ion beam

induced damage which caused an increasing dark current with beam fluence compare to linear mode.

We also tested an APD device SPAD50 (photo in Figure 4), which has a similar high field zone at the centre n^+ contact disk, but has no guard-ring around the n^+ contact electrode edge. This device functioned well in linear mode we obtained an IBIC map at 80 K with the maximum allowed bias voltage before breakdown, as displayed in Figure 4. In this case 100% charge collection efficiency (gain=1) was achieved at the centre area, and 140% charge collection efficiency (gain=1.4) was observed for an area surrounding the edge of the n^+ contact electrode indicating charge gain from internal avalanche processes. Here, the localized high field at the electrode edge was responsible for the avalanche process but without a guard-ring the device was vulnerable to breakdown when biased into Geiger mode.

3. DISCUSSION

In the APD device (SHV1150) in Figure 3, the e-h pairs generated within the center n^+ contact, which is the high field avalanche zone, can develop enough momentum during drift to make ionization impacts which result in the charge multiplication effect. However, the very short drift distance to the field termination electrode limits the final momentum, therefore the charge gain only increases slowly with bias voltage and saturates at a low value of 1.4 when the APD is operated in linear mode. Previously, we made a detailed study on the correlation between the APD's charge gain and the structure of avalanche zone [Yang 2010]. We found that if the avalanche zone is constructed very close to the surface, the resulting charge gain saturates at a value similar to that observed here. To achieve a high charge gain while maintaining a low leakage current requires the avalanche zone to be fabricated at the back side of the device. This provides sufficient drift distance for the charge carriers from the ion impact on the surface to build-up momentum for the ionization cascade that creates the avalanche and hence the charge gain. In Figure 3, the e-h pairs created by the impact of single ions at the location between the p^+ contact and guard-ring cannot reach a high enough

momentum to trigger an avalanche and are terminated at the guard-ring resulting in unity gain just as for a normal p-i-n structure. Without a guard-ring, the APD SPAD050 had a relatively high electrical field around the n^+ contact edge, in which the higher charge gain (gain=1.4) was obtained in the linear mode of operation. Higher gain is possible in principle by raising the bias voltage however for this device further increases of the bias voltage caused the local dielectric to break down and resulted in a large noise output. For stable Geiger mode operation, a guard-ring surrounding the avalanche zone's electrode is essential.

4. CONCLUSION

We tested APD devices in both Geiger mode (Gain>1000) and linear mode (Gain=1, and >1) at maximum allowed DC bias voltage by imaging the collected charge. For our applications both modes of operation are suitable for the deterministic doping of silicon substrates provided the incident beam fluence rate, delay time and substrate temperature are suitably optimised for the device characteristics. A suitable guard-ring is essential for reliable operation of APD devices in Geiger mode.

ACKNOWLEDGEMENTS

The authors acknowledge the assistance of Roland Szymanski at the University of Melbourne for performing the IBIC measurements and of Daniel Spemann for useful discussions. This research was funded by the Australian Research Council Centre of Excellence for Quantum Computation and Communication Technology (project number CE11E0001027) and the US Army Research Office (W911NF-13-1-0024).

REFERENCES

[Akiba 2005] M. Akiba, M. Fujiwara, and M. Sasaki, Opt. Lett. 30 (2005) 123.

[Andresen 2000] S. E. S. Andresen, R. Brenner, C. Wellard, C. Yang, T. F. Hopf, C. C. Escott, R. G. Clark, A. S. Dzurak, D. Jamieson and L. Hollenberg, Nano Letters 7 (2007) 2000.

[Baron 2000] Alfred Q. R. Baron, Hyperfine Interactions 125 (2000) 29.

[Bielejec 2010] E. Bielejec, J. A. Seamons, M. S. Carroll, Nanotechnology 21, 085201 (2010).

[Bugge 2014] Audun Nystad Bugge, Sebastien Sauge, Aina Mardhiyah M. Ghazali, Johannes Skaar, Lars Lydersen, and Vadim Makarov, Phys. Rev. Lett. 112, 070503-1 (2014).

[Campbell 2007] J. C. Campbell, Journal of Light wave Technology 25 (2007) 109.

[Ghioni 2007] M. Ghioni, A. Gulinatti, I. Rech, F. Zappa, S. Cova, IEEE Journal of Selected Topics in Quantum Electronics 13 (2007) 852.

[Hudson 2008] F.E. Hudson, A.J. Ferguson, C. C. Escott, C. Yang, D. Jamieson, R. G. Clark and A. S. Dzurak, Nanotechnology 19 (2008) 1954021.

[Hughes 2002] R. J. Hughes, J. E. Nordholt, D. Derkacs, and C.G. Peterson, New J. Phys. 4, 43 (2002).

[Jamieson 2005] D. N. Jamieson, C. Yang, T. Hopf, S. M. Hearne, C. I. Pakes, S. Prawer, M. Mitic, E. Gauja, S. E. Andresen, F. E. Hudson, A. S. Dzurak, and R. G. Clark, Appl. Phys. Lett. 86 (2005) 202101.

[Kishimoto 2000] S. Kishimoto et al., Phys. Rev. Lett. 83 (2000) 1831.

[Kurtsiefer 2002] C. Kurtsiefer, P. Zarda, M. Halder, H. Weinfurter, P.M. Gorman, P. R. Tapster, and J. G. Rarity, Nature (London) 419, 450 (2002).

[Mitic 2006] M. Mitic, M. C. Cassidy, K. D. Petersson, R. P. Starrett, E. Gauja, R. Brenner, R. G. Clark, A. S. Dzurak, C. Yang and D. Jamieson, Applied Physics Letters. 89 (2006) 0135031.

[Morello 2010] A. Morello, J. J. Pla, F. A. Zwanenburg, K. W. Chan, K. Y. Tan, H. Huebl, M. Mottonen, C. D. Nugroho, C. Y. Yang, J. A. van Donkelaar, A. D. C. Alves, D. N. Jamieson, C. C. Escott, L. C. L. Hollenberg, R. G. Clark and A. S. Dzurak, Nature 467 (7316), 687-691 (2010).

[Pelso 2009] M. P. Peloso, I. Gerhardt, C. Ho, A. Lamas-Linares, and C. Kurtsiefer, New J. Phys. 11, 045007 (2009).

[Poppe 2004] A. Poppe, A. Fedrizzi, R. Ursin, H. R. Böhm, T. Loünser, O. Maurhardt, M. Peev, M. Suda, C. Kurtsiefer, H. Weinfurter, T.Jennewein, and A. Zeilinger, Opt. Express 12, 3865 (2004).

[Schmitt-Manderbach 2007] T. Schmitt-Manderbach, H. Weier, M. Fürst, R. Ursin, F. Tiefenbacher, T. Scheidl, J. Perdigues, Z. Sodnik, C. Kurtsiefer, J. G. Rarity, A. Zeilinger, and H. Weinfurter, Phys. Rev. Lett. 98, 010504 (2007).

[Seamons 2008] J. A. Seamons, E. Bielejec, M. S. Carroll, and K. D. Childs, Appl. Phys. Lett. 93 (2008) 043124.

[Tsujino 2007] Kenji Tsujino, Makoto Akiba, and Masahide Sasaki, Applied Optics 46 (2007) 1009.

[Yang 2010] C. Y. Yang and D. Jamieson, Nuclear Instruments & Methods in Physics Research Section B-Beam Interactions with Materials and Atoms 268 (11-12), 2034-2037 (2010).

Figure Captions

Figure 1: Systematic layout of circuit diagrams for the two modes of APD operation for single ion detection in a Nuclear Microprobe: (a) Geiger mode and (b) linear mode. Both modes use pulsed ion beam to control the original beam current ~ 1pA; with pulsed beam duration 1 microsecond and cycle frequency 100 Hz.

Figure 2: Synchronized pulses (ch-1 and ch-2) are sent individually to bias the APD and to a beam deflector for a beam-on-demand control. The Geiger signal shown generated from a single ion strike in the APD device is within the time window of the Geiger mode activation created by superimposing the bias voltage pulse (ch-1) with the permanent APD's DC bias voltage. The APD bias pulse is tuned to delay a period of time Δt with respect to the beam gate to account for ion traveling from the beam deflector to the target device.

Figure 3: APD device (SHV1150) analyzed with linear IBIC and Geiger mode imaging operation. The n+ contact has a diameter about 630 micrometers and around its outer edge there is guard-ring for preventing a localized break-down. The charge multiplication with low gain avalanching was achieved at the high electrical field area under the n^+ contact, with IBIC showing 140% (charge gain=1.4) relative charge collection efficiency. The e-h pairs created by single ions at the location between the p^+ contact and guard-ring can not reach a momentum high enough to make ionization impact and terminated at the guard-ring resulting in 100% charge collection

Figure 4: Photo and linear mode IBIC image from an APD device SPAD050. The APD has no guard-ring surrounding the n^+ contact electrode edge. It was not possible to obtain any clear Geiger mode

imaging due to the presence of high noise signals. The linear mode operation with the maximum allowed bias voltage at 80 K produced 100% charge collection efficiency (gain=1) at the centre area, and 140% charge collection efficiency (gain=1.4) in a ring surrounding the edge of the n^+ contact electrode.

FIGURES

Figure 1

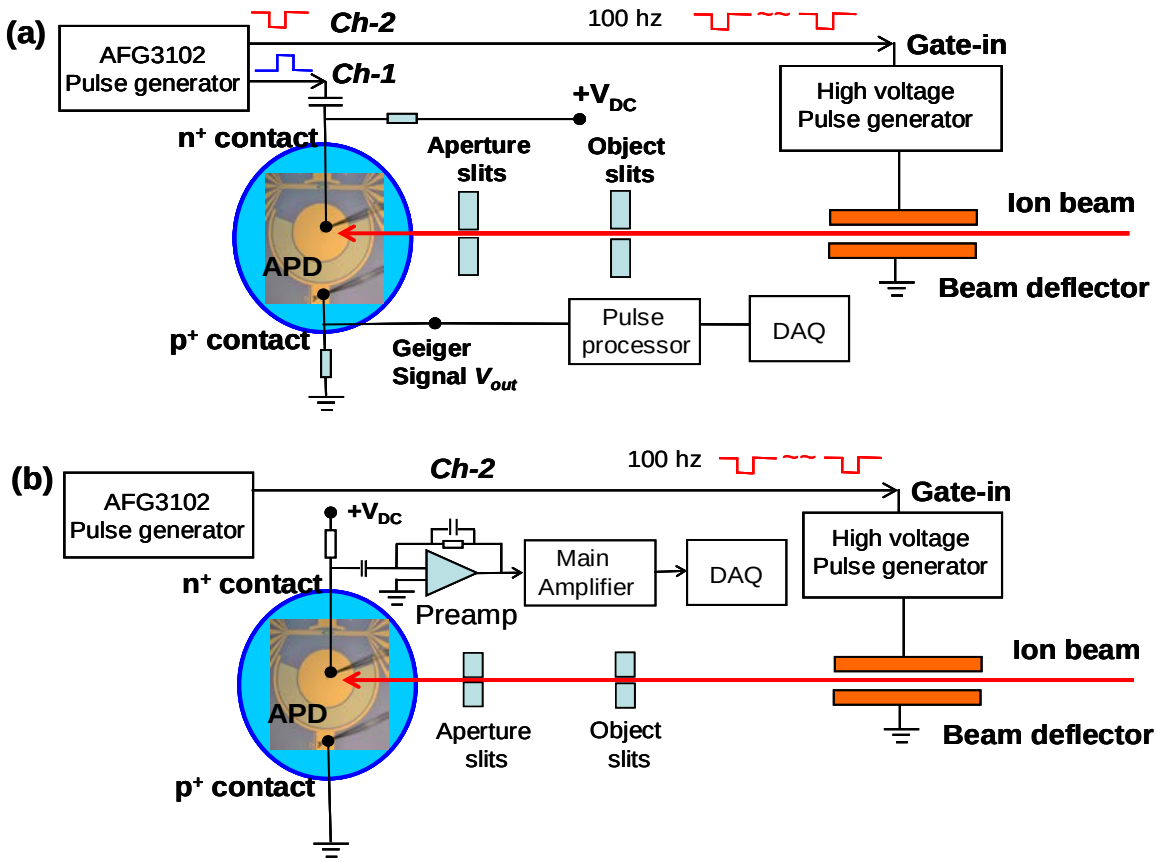

Figure 2

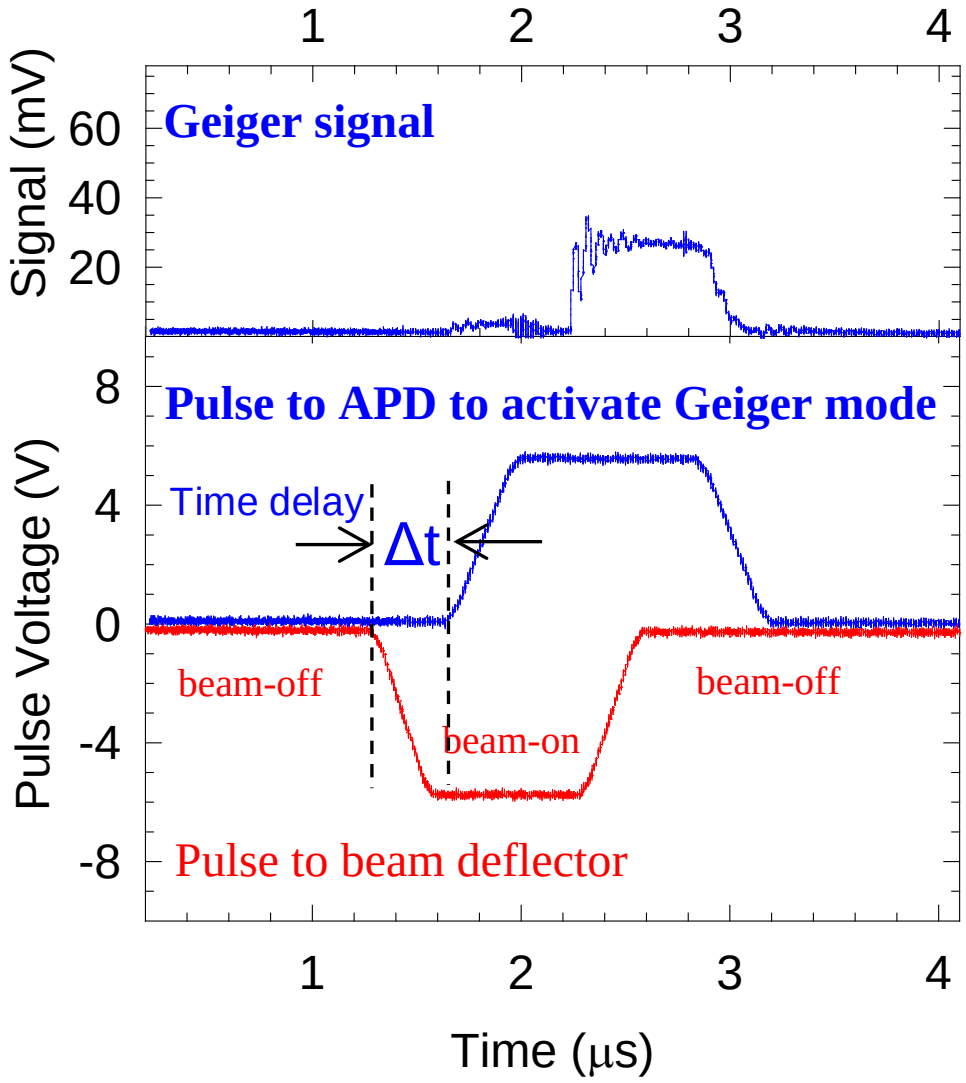
Geiger signal
Signal (mV)
60
40
20
Pulse to APD to activate Geiger mode
Time delay
Δt
beam-off
beam-on
beam-off
Pulse to beam deflector
Pulse Voltage (V)
8
4
0
-4
-8
1
2
3
4
Time (μs)

Figure 3

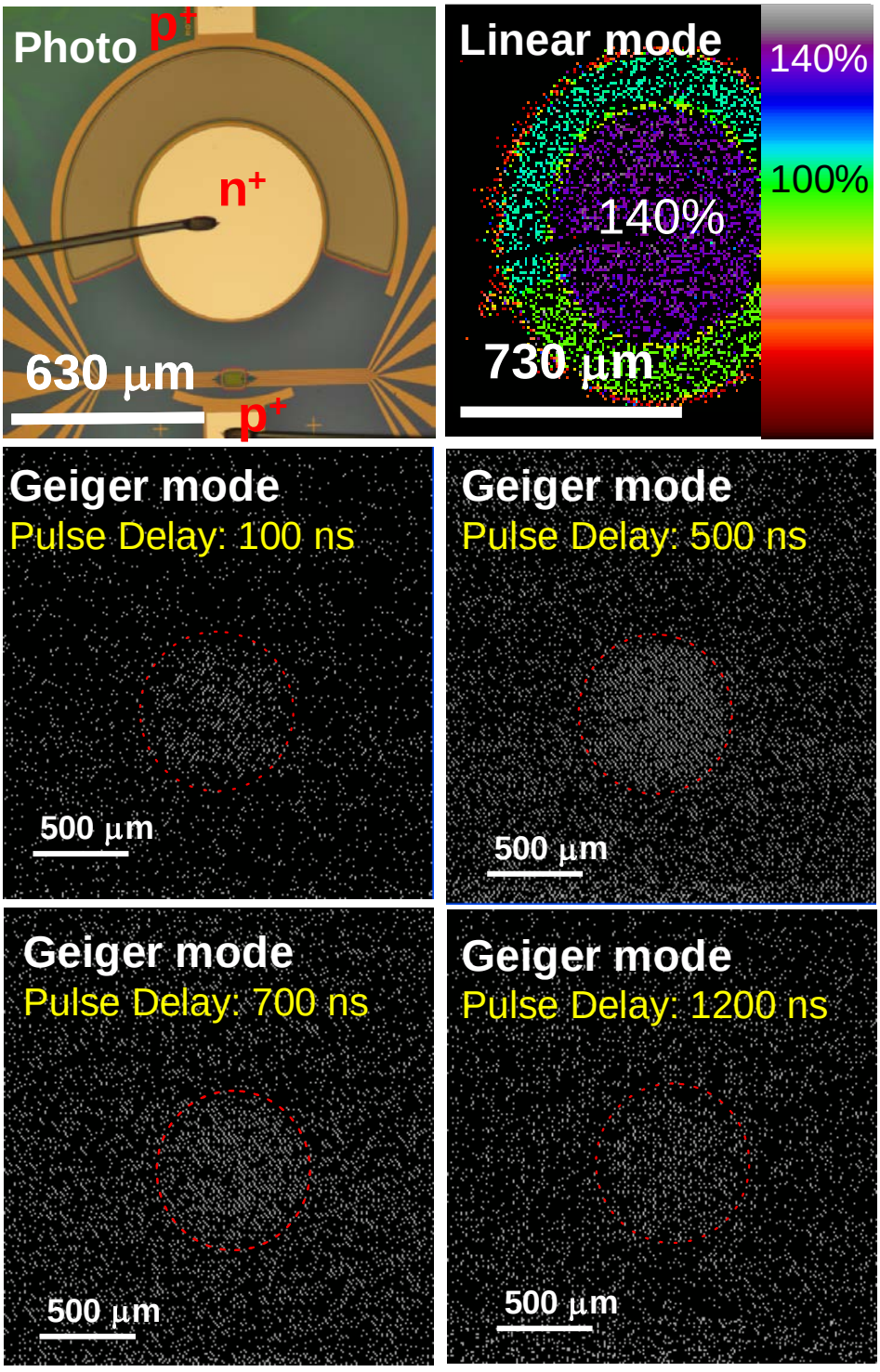
Photo
p+
n+
630 μm
p+
Linear mode
140%
100%
140%
730 μm
Geiger mode
Pulse Delay: 100 ns
500 μm
Geiger mode
Pulse Delay: 500 ns
500 μm
Geiger mode
Pulse Delay: 700 ns
500 μm
Geiger mode
Pulse Delay: 1200 ns
500 μm

Figure 4